ACS OMEGA

Open Access



http://pubs.acs.org/journal/acsodf

Article

# Identification of Potential Tryptase Inhibitors from FDA-Approved Drugs Using Machine Learning, Molecular Docking, and Experimental Validation

Muhammad Yasir, Jinyoung Park, Eun-Taek Han, Won Sun Park, Jin-Hee Han, and Wanjoo Chun*

Cite This: *ACS Omega* 2024, 9, 38820−38831

Read Online

ACCESS | Metrics & More | Article Recommendations | Supporting Information

**ABSTRACT:** This study explores the innovative use of machine learning (ML) to identify novel tryptase inhibitors from a library of FDA-approved drugs, with subsequent confirmation via molecular docking and experimental validation. Tryptase, a significant mediator in inflammatory and allergic responses, presents a therapeutic target for various inflammatory diseases. However, the development of effective tryptase inhibitors has been challenging due to the enzyme's complex activation and regulation mechanisms. Utilizing a machine learning model, we screened an extensive FDA-approved drug library to identify potential tryptase inhibitors. The predicted compounds were then subjected to molecular docking to assess their binding affinity and conformation within the tryptase active site. Experimental validation was performed using RBL-2H3 cells, a rat basophilic leukemia cell line, where the efficacy of these compounds was evaluated based on their ability to inhibit tryptase activity and suppress $\beta$-hexosaminidase activity and histamine release. Our results demonstrated that several FDA-approved drugs, including landiolol, laninamivir, and cidofovir, significantly inhibited tryptase activity. Their efficacy was comparable to that of the FDA-approved mast cell stabilizer nedocromil and the investigational agent APC-366. These findings not only underscore the potential of ML in accelerating drug repurposing but also highlight the feasibility of this approach in identifying effective tryptase inhibitors. This research contributes to the field of drug discovery, offering a novel pathway to expedite the development of therapeutics for tryptase-related pathologies.

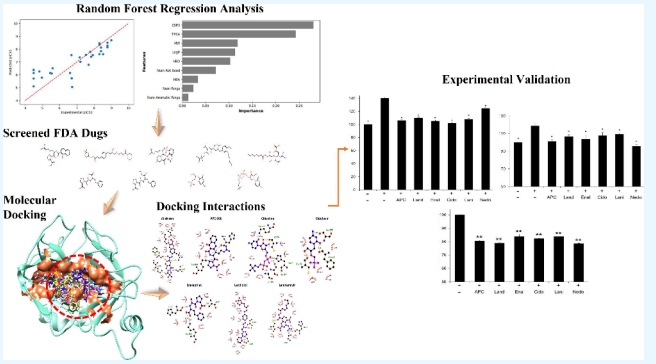


## INTRODUCTION

Mast cells are central to the body's immune response to external antigens and are predominantly found in vascularized tissues such as the mucosal and epithelial layers of the gastrointestinal tract, skin, and respiratory tract.[1−3] These cells, when activated by various stimuli, release a range of inflammatory mediators from their cytoplasmic granules.[4] This release can lead to the development of various inflammatory disorders, including asthma, atopic dermatitis, and severe anaphylactic shock.[5−7] Among the diverse molecules stored in these granules are histamine, heparin, cytokines, and a spectrum of proteases, with tryptase being the most abundant protease present in human mast cells.[8]

Tryptase, a member of the trypsin family of proteases, is a tetrameric enzyme. It is composed of four catalytic subunits that together form a distinctive ring-like structure, with the active sites facing an oval-shaped central pore.[9] This unique structural arrangement is crucial for its biological function. The role of tryptase in inflammatory and allergic responses has been extensively documented, highlighting its significance as a potential therapeutic target for a variety of inflammatory diseases.[10−12] Its involvement in biological processes such as fibrosis, angiogenesis, and immune response modulation further emphasizes its clinical importance.[5,13] Despite the critical role of tryptase in these processes, the development of effective inhibitors has been a complex challenge, mainly due to the intricate mechanisms governing its activation and regulation.[13] Addressing this challenge requires a nuanced understanding of tryptase's structure and function, as well as innovative approaches to inhibit its activity.

Given the complexity and resource-intensive nature of developing new drugs, drug repurposing, also known as drug repositioning, emerges as a promising strategy.[14,15] Drug repurposing involves identifying new therapeutic applications for already approved drugs beyond their original intended uses.[16] This approach can significantly accelerate the drug development process, augmenting the value of existing drugs

Received: May 24, 2024
Revised: August 23, 2024
Accepted: August 29, 2024
Published: September 4, 2024

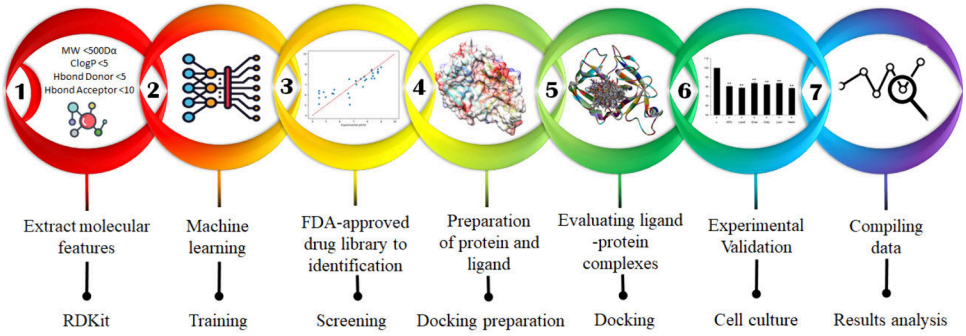


**Figure 1.** Workflow diagram of the predicted research study.

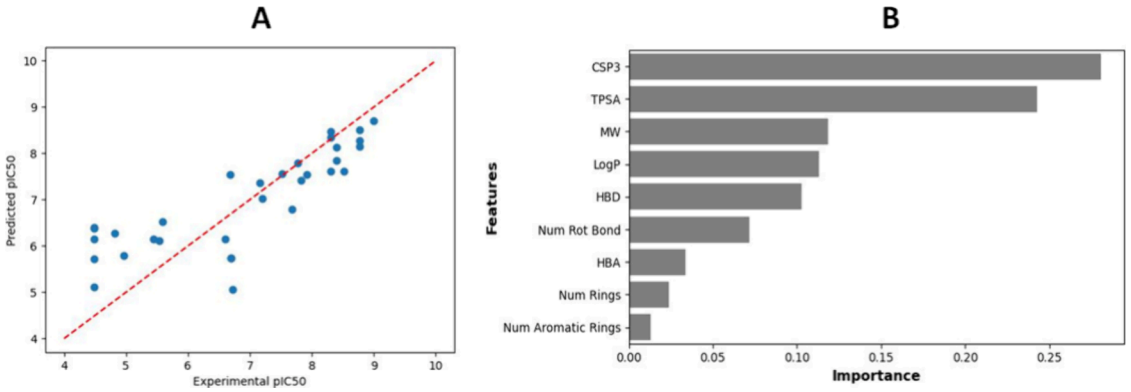


**Figure 2.** (A) Correlation of experimental pIC50 values with predicted pIC50 values with the regression model. (B) Illustration of the feature importance values.

and potentially offering new treatment avenues for diseases that currently lack effective therapies.[17,18] Importantly, in the context of tryptase inhibitors, drug repurposing can provide new treatments for inflammatory diseases, aligning with the need for efficient and rapid therapeutic development. This approach holds significant potential in addressing unmet medical needs related to tryptase-related conditions.

Computational study, or computer-aided drug design (CADD), is now a crucial component in drug discovery and development.[19−21] CADD utilizes computational methods and software for rapid and efficient screening of large compound libraries, offering a more time- and cost-effective alternative to traditional experimental approaches.[22,23] This approach dramatically reduces the need for synthesizing and experimentally testing numerous compounds, allowing for the virtual screening of thousands of compounds.

Machine learning (ML), a subset of artificial intelligence, is another transformative force in drug development.[24] It enables computers to learn from data, predict outcomes, and make decisions autonomously.[25] ML excels in analyzing vast and complex data sets, identifying new drug targets, predicting drug efficacy, and optimizing drug properties. Within the sphere of machine learning techniques utilized in drug discovery, the Random Forest regression algorithm stands out for its efficacy and reliability.[26−28] This algorithm operates by constructing a multitude of decision trees during training and outputting the mean prediction of the individual trees. This ensemble approach makes it exceptionally good at handling large data sets with numerous input variables, a common scenario in drug development. Random Forest is particularly adept at identifying complex, nonlinear relationships within data, making it suitable for predicting drug efficacy and toxicity. Its robustness against overfitting, even with relatively small data sets, is a significant advantage in the early stages of drug discovery.[29,30] Moreover, the algorithm provides insights into feature importance, enabling researchers to identify key molecular descriptors and biological properties that are most predictive of a drug's performance.[31]

In this study, we employed an ML-based model, trained using a reference library of known tryptase inhibitors, to screen an FDA-approved drug library to identify potential tryptase inhibitors. The candidate compounds were further analyzed using molecular docking. Subsequent biological examination was conducted to validate these candidates. This approach, leveraging drug repositioning, has the potential to yield novel tryptase inhibitors, contributing significantly to the field of inflammatory disease treatment.

## RESULTS AND DISCUSSION

Figure 1 illustrates the workflow that integrates machine learning algorithms, molecular docking experiments, and experimental validation approaches for drug repurposing of novel tryptase inhibitors. The study followed a seven-step process: (1) Extraction of molecular features from the reference data set using RDKit, (2) Training of machine learning algorithm, (3) Screening of an FDA-approved drug library to identify lead compounds, (4) Retrieval of tryptase 3D structure and preparation of ligands, (5) Conducting molecular docking for ligand-protein complexes, (6) Experimental validation of candidates through cell culture studies, (7) Analysis of results to assess the performance of repositioning of FDA-approved drug candidates as novel tryptase inhibitors.


https://doi.org/10.1021/acsomega.4c04886
ACS Omega 2024, 9, 38820−38831

Table 1. Comprehensive Details Regarding Drugs That Were Predicted by the Random Forest Regression Model to Possess High Potential for Tryptase Inhibition

| No. | Name | MW | LogP | HBA | HBD | CSP3 | R-Bounds[a] | Rings[b] | TPSA | A-Rings[c] | predicted pIC50 |
|---|---|---|---|---|---|---|---|---|---|---|---|
| 1 | Meropenem trihydrate | 437.18 | −2.78 | 11 | 9 | 0.71 | 5 | 3 | 204.68 | 0 | 8.926 |
| 2 | Doripenem hydrate | 438.12 | −2.43 | 11 | 8 | 0.73 | 7 | 3 | 193.56 | 0 | 8.896 |
| 3 | D-Amygdalin | 457.16 | −3.11 | 12 | 7 | 0.65 | 7 | 3 | 202.32 | 1 | 8.855 |
| 4 | Zanamivir | 332.13 | −3.58 | 11 | 9 | 0.58 | 6 | 1 | 198.22 | 0 | 8.707 |
| 5 | Cidofovir dihydrate | 315.08 | −3.31 | 11 | 9 | 0.50 | 6 | 1 | 210.90 | 1 | 8.652 |
| 6 | Aztreonam | 435.05 | −1.17 | 13 | 5 | 0.46 | 7 | 2 | 201.58 | 1 | 8.621 |
| 7 | Aliskiren | 551.39 | 3.29 | 9 | 6 | 0.73 | 19 | 1 | 146.13 | 1 | 8.606 |
| 8 | Citicoline | 488.11 | −2.23 | 15 | 5 | 0.71 | 10 | 2 | 215.72 | 1 | 8.569 |
| 9 | Cefminox sodium | 541.05 | −6.17 | 14 | 4 | 0.56 | 11 | 3 | 205.69 | 1 | 8.566 |
| 10 | Laninamivir octanoate | 472.25 | −0.22 | 12 | 7 | 0.71 | 14 | 1 | 195.79 | 0 | 8.561 |
| 11 | Omacetaxine mepesuccinate | 545.26 | 2.58 | 10 | 2 | 0.66 | 9 | 5 | 123.99 | 1 | 8.559 |
| 12 | Oleuropein | 540.18 | −0.63 | 13 | 6 | 0.52 | 9 | 3 | 201.67 | 1 | 8.557 |
| 13 | Argatroban monohydrate | 526.26 | 0.09 | 12 | 9 | 0.61 | 9 | 3 | 209.21 | 1 | 8.547 |
| 14 | Gilteritinib | 552.35 | 2.70 | 11 | 4 | 0.62 | 9 | 5 | 121.11 | 2 | 8.524 |
| 15 | Cinitapride tartrate | 552.24 | 1.00 | 14 | 7 | 0.56 | 10 | 3 | 225.79 | 1 | 8.470 |
| 16 | Paeoniflorin | 480.16 | −1.36 | 11 | 5 | 0.70 | 6 | 8 | 164.37 | 1 | 8.461 |
| 17 | Naringin | 580.18 | −1.17 | 14 | 8 | 0.52 | 6 | 5 | 225.06 | 2 | 8.456 |
| 18 | Tofacitinib citrate | 504.20 | 0.30 | 14 | 5 | 0.50 | 8 | 3 | 221.04 | 2 | 8.422 |
| 19 | Citicoline sodium | 510.09 | −5.86 | 15 | 4 | 0.71 | 10 | 2 | 218.55 | 1 | 8.400 |
| 20 | Acotiamide hydrochloride hydrate | 540.20 | 0.91 | 12 | 9 | 0.48 | 10 | 2 | 207.52 | 2 | 8.393 |
| 21 | Argatroban | 508.25 | 0.91 | 11 | 7 | 0.61 | 9 | 3 | 177.71 | 1 | 8.361 |
| 22 | Puromycin 2HCl | 543.18 | 0.05 | 12 | 5 | 0.45 | 8 | 4 | 160.88 | 3 | 8.355 |
| 23 | Chloroquine phosphate | 515.14 | 2.95 | 11 | 7 | 0.50 | 8 | 2 | 183.68 | 2 | 8.349 |
| 24 | Gadodiamide hydrate | 574.10 | −7.37 | 13 | 2 | 0.69 | 16 | 0 | 188.31 | 0 | 8.347 |
| 25 | Harpagoside | 494.18 | −1.20 | 11 | 6 | 0.54 | 6 | 4 | 175.37 | 1 | 8.345 |
| 26 | Darunavir | 547.24 | 2.38 | 10 | 4 | 0.52 | 11 | 4 | 140.42 | 2 | 8.334 |
| 27 | Terbutaline sulfate | 548.24 | 2.39 | 12 | 10 | 0.50 | 6 | 2 | 220.04 | 2 | 8.331 |
| 28 | Fludarabine phosphate | 365.05 | −1.72 | 12 | 6 | 0.50 | 4 | 3 | 186.07 | 2 | 8.330 |
| 29 | Ribociclib succinate | 552.28 | 2.73 | 13 | 4 | 0.48 | 8 | 5 | 165.81 | 3 | 8.324 |
| 30 | Vardenafil hydrochloride trihydrate | 578.23 | 0.02 | 13 | 7 | 0.52 | 8 | 4 | 207.40 | 3 | 8.322 |
| 31 | Doripenem | 420.11 | −1.60 | 10 | 6 | 0.73 | 7 | 3 | 162.06 | 0 | 8.307 |
| 32 | Naringin dihydrochalcone | 582.19 | −1.35 | 14 | 9 | 0.52 | 9 | 4 | 236.06 | 2 | 8.277 |
| 33 | Enalaprilat dihydrate | 384.19 | −0.52 | 9 | 7 | 0.50 | 8 | 2 | 169.94 | 1 | 8.273 |
| 34 | Landiolol hydrochloride | 545.25 | 1.11 | 11 | 3 | 0.68 | 13 | 3 | 127.82 | 1 | 8.259 |
| 35 | Iopamidol | 776.85 | −1.01 | 11 | 8 | 0.47 | 10 | 1 | 188.45 | 1 | 8.251 |
| 36 | Harringtonine | 531.25 | 2.19 | 10 | 2 | 0.64 | 8 | 5 | 123.99 | 1 | 8.248 |
| 37 | Medihaler-ISO | 556.23 | −0.04 | 14 | 14 | 0.45 | 8 | 2 | 283.04 | 2 | 8.231 |
| 38 | Ioversol | 806.86 | −2.02 | 12 | 8 | 0.50 | 12 | 1 | 199.89 | 1 | 8.223 |
| 39 | Iohexol | 820.88 | −1.63 | 12 | 8 | 0.53 | 12 | 1 | 199.89 | 1 | 8.223 |
| 40 | Atosiban | 993.44 | −3.04 | 23 | 14 | 0.63 | 18 | 3 | 365.67 | 1 | 8.223 |
| 41 | Carbetocin (acetate) | 1047.51 | −2.41 | 25 | 14 | 0.62 | 18 | 3 | 399.81 | 1 | 8.222 |
| 42 | Gadodiamide | 592.11 | −8.19 | 14 | 4 | 0.69 | 16 | 0 | 219.81 | 0 | 8.221 |
| 43 | Doxorubicin | 543.17 | 0.00 | 12 | 7 | 0.44 | 5 | 5 | 206.07 | 2 | 8.220 |
| 44 | Oxytocin acetate | 1066.46 | −3.52 | 26 | 17 | 0.60 | 17 | 3 | 436.83 | 1 | 8.202 |

[a]Number of rotatable bonds. [b]Number of rings. [c]Number of aromatic rings.

## MACHINE LEARNING REGRESSION ANALYSIS OF THE TRYPTASE REFERENCE DATA SET

Utilizing the RDKit toolkit, nine distinct molecular descriptors were computed for a data set of 168 compounds, known as the tryptase reference data set. This data set was subsequently partitioned into a training set and a test set, with the training set comprising 80% of the data, and the remaining 20% split evenly between two test sets (8:1:1). The training set was then subjected to Random Forest Regression to develop a predictive model. The model's performance was assessed by applying it to the test set of the tryptase reference data set. In Figure 2A, a visual representation is provided that illustrates the relationship between the experimentally determined pIC50 values and those predicted by a custom-built regression model. The assessment of this regression model's accuracy was conducted by computing the Mean Squared Error (MSE) and the regression coefficient, utilizing the scikit-learn library. The analysis yielded an MSE of 0.806 and a regression coefficient of 0.83. Considering the inherent variability in pIC50 values, which stem from diverse experimental methodologies, these metrics were deemed acceptable.

## MOLECULAR DESCRIPTOR'S CONTRIBUTION IN REGRESSION PREDICTION

To gain insight into the influence of individual descriptors on the regression model, the Random Forest Regression tool was



https://doi.org/10.1021/acsomega.4c04886
ACS Omega 2024, 9, 38820−38831

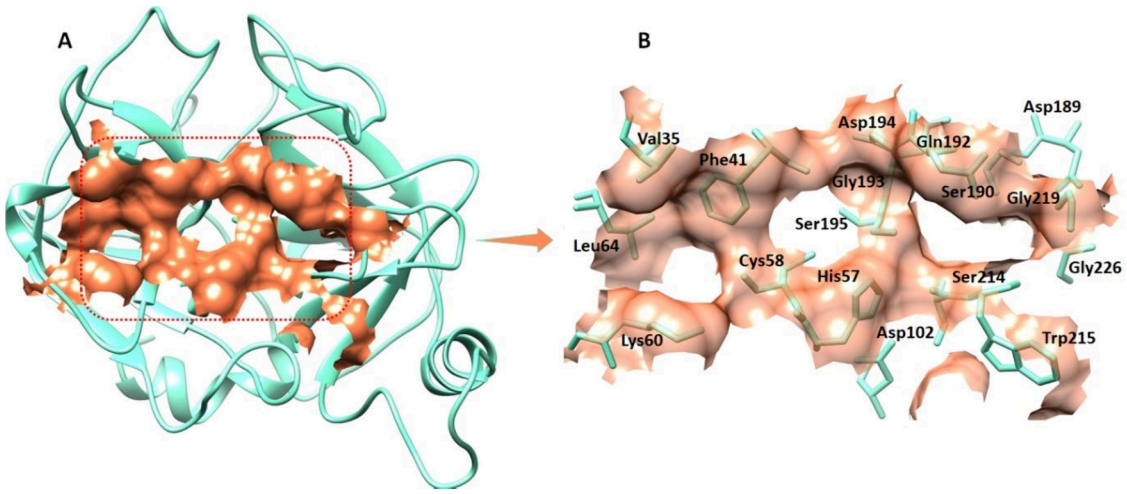


**Figure 3.** (A) This panel shows the spatial positioning of the tryptase active site. The enzyme's structure is represented as a ribbon in aquamarine, with the binding site surface highlighted in coral. (B) This panel focuses on the key residues within the active region of tryptase, crucial for ligand binding. Notably, the catalytic triad, consisting of His57, Asp102, and Ser195, is highlighted to emphasize its role in the enzyme's activity. Additional crucial amino acids for ligand binding, including Gly193, Ser195, Asp194, Ser214, Ser190, and Asp189, are also emphasized.

employed to determine the importance of each feature. Feature importance serves as an indicator of the extent to which each descriptor affects the model's predictive accuracy. Descriptors with greater importance scores are deemed to have a more significant effect on the pIC50 prediction, whereas those with lower scores are considered to have a lesser impact. Among nine molecular descriptors evaluated, including molecular weight, LogP value, counts of hydrogen bond donors and acceptors, the proportion of sp3 hybridized carbon atoms (CSP3), the number of aromatic bonds, ring count, topological polar surface area (TPSA), and the number of aromatic rings, the CSP3 descriptor emerged as the most influential in predicting pIC50 values. Following closely in importance were the TPSA and molecular weight descriptors (Figure 2B).

## PREDICTION OF PIC50 VALUES OF FDA-APPROVED DRUG LIBRARY DATA SET

Following the development of the regression model using the tryptase reference data set, the prediction of the pIC50 value of an FDA-approved drug library data set was carried out. The molecular descriptors of 3,105 drugs were computed utilizing the RDKit toolkit. The regression model was utilized to predict pIC50 values by applying the data set of molecular features from the FDA-approved drug library. The predictions for FDA-approved drugs ranged from 4.676 M to 8.926. Drugs predicted to have high pIC50 values, specifically those above 8.2, are detailed in Table 1. To delve deeper into the effectiveness of these compounds in inhibiting tryptase, molecular docking studies and molecular dynamics (MD) simulations were conducted with the compounds having predicted pIC50 values of greater than 8.0, which corresponds to 10 nM in IC50 values. Considering the absence of any FDA-approved tryptase inhibitors, APC-366, a compound currently under investigation as a tryptase inhibitor, was used as a positive reference in computational and experimental evaluations.

## STRUCTURAL ANALYSIS OF THE TRYPTASE PROTEIN

Tryptase holds the distinction of being the most abundant serine proteinase derived from secretory granules within mast cells. Its presence has been utilized as a marker for mast cell activation.[32] It is made up of 245 amino acids forming a single chain (PDBID: 2GDD). The protein exhibits a complex structure involving loops, $\alpha$-helices, and $\beta$-sheets, contributing to its overall conformation. Furthermore, a VADAR 1.8 structural study revealed that tryptase is made up of 8% $\alpha$-helices, 45% $\beta$-sheets, 46% coils, and 30% turns. Based on the Ramachandran plots, 94.6% of amino acids were situated within the favored region, while 100% of residues fall within the allowed zone of dihedral angles phi ($\varphi$) and psi ($\psi$) (Figure S1).

## THE BINDING POCKET ANALYSIS

The functional attributes of a binding pocket are influenced not only by its geometry and position within a protein but also by the particular amino acid residues that encircle it.[33] In this study, the binding pocket residues were identified using the Discovery Studio ligand interaction approach, and compared to already available data (PBID: 2GDD) revealing Val35, Phe41, Cys58, Lys60, Leu64, Asp189, Gln192, Gln195, Ser214, Trp215, Gly219, and Gly226 as the active site amino acid residues. The cocrystallized ligand was utilized to construct the binding sphere, focusing on our selected binding pocket residues the sphere was contracted. Therefore, the sphere's dimensions were adjusted to X = 13.4387, Y = 57.5649, and Z = 70.0616, with a fixed radius of 11.3075. These parameters were set to investigate the interaction of screened compounds against the tryptase active site (Figure 3).

## MOLECULAR DOCKING ANALYSIS

The CDocker module within Discovery Studio was employed to forecast negative energy values, specifically CDocker energy and CDocker interaction energy. CDocker energy encapsulates the overall docking energy, which is derived from the 3D structural and physiochemical attributes of both the ligand and the protein. In contrast, CDocker interaction energy focuses


https://doi.org/10.1021/acsomega.4c04886
ACS Omega 2024, 9, 38820−38831

Table 2. Overall Docking Energy and Interaction Energy Values (in kcal/mol) of Complexes and the Targets of These Drugs

| Drugs | CDocker energy (kcal/mol) | CDocker interaction energy (kcal/mol) | Target/action |
|---|---|---|---|
| Gadodiamide | −66.491 | −38.111 | contrast agent used in MRI scan |
| Landiolol | −52.838 | −61.482 | beta1 adrenergic receptor antagonist, antihypertensive |
| Argatroban | −49.084 | −48.664 | thrombin inhibitor, anticoagulant |
| Aliskiren | −47.394 | −61.147 | renin inhibitor, antihypertensive |
| Medihaler-ISO | −44.864 | −37.333 | isoproterenol, beta-receptor agonist, asthma |
| Laninamivir octanoate | −43.290 | −51.591 | neuraminidase (NA) inhibitor, anti-influenza virus |
| Enalaprilat | −40.231 | −39.708 | angiotensin-converting enzyme inhibitor, antihypertensive |
| Cidofovir dihydrate | −39.702 | −40.036 | inhibitor of human herpesviruses, antiviral |
| Citicoline | −37.610 | −51.855 | cytidine-5′-diphosphocholine, dietary supplement |
| Iopamidol | −35.248 | −50.141 | iodinated contrast agent |
| Imidazolidinyl urea | −35.072 | −44.732 | antimicrobial preservative in cosmetics |
| Uridine 5′-triphosphate | −34.573 | −40.722 | UTP |
| Adenosine-5′-triphosphate | −32.161 | −51.503 | ATP |
| Calcium D-Panthotenate | −28.740 | −30.830 | treatment of deficiency of pantothenic acid |
| APC_366 | −27.447 | −41.574 | selective inhibitor of mast cell tryptase (investigational) |
| Puromycin 2HCl | −26.928 | −49.088 | aminonucleoside antibiotic |
| Vardenafil hydrochloride | −26.385 | −43.237 | phosphodiesterase 5 inhibitor, erectile dysfunction |
| Adenosine-5′-diphosphate | −25.095 | −38.643 | ADP |
| Fludarabine phosphate | −24.216 | −36.459 | purine analogue and antineoplastic agent, anticancer |
| Ioversol | −22.914 | −45.552 | iodinated contrast agent |
| Adenosine 5′-monophosphate | −22.303 | −36.508 | AMP |
| Doxorubicin | −21.817 | −44.790 | anthracycline group of chemotherapeutic agent |
| Chloroquine | −21.094 | −36.407 | antimalarial |
| Gilteritinib | −21.007 | −55.575 | FLT3 (receptor tyrosine kinase) inhibitor, antileukemia |
| APC_2059 | −20.488 | −78.151 | selective inhibitor of mast cell tryptase (investigational) |

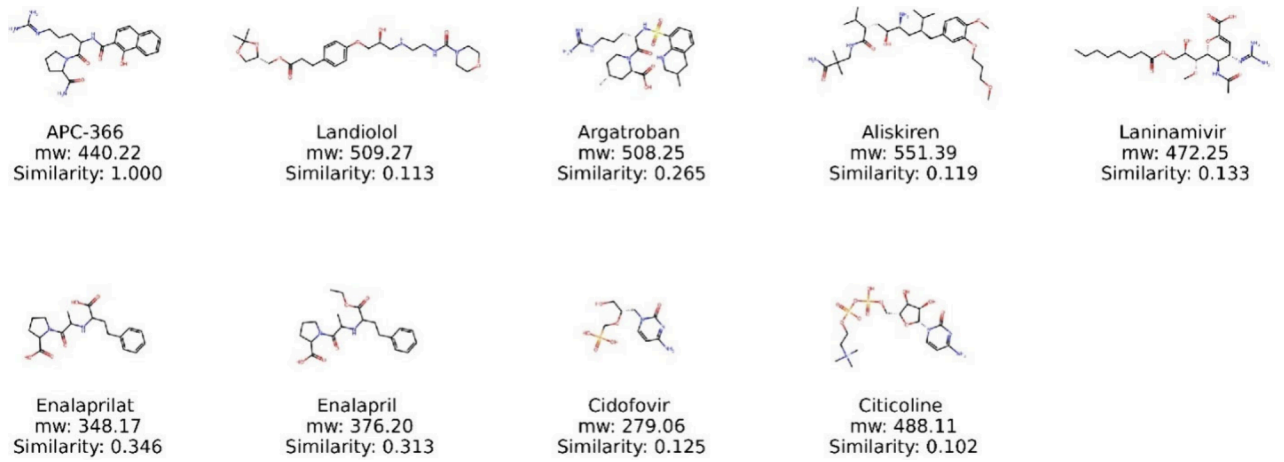


**Figure 4.** Structures of highly predicted tryptase inhibitors from molecular docking with the reference compound of APC-366.

exclusively on the energy related to the interactions between the ligand and the receptor. This encompasses the contributions from various intermolecular forces, such as van der Waals forces, electrostatic complementarity, and hydrogen bonding, all of which contribute to the binding affinity. CDocker Interaction Energy provides a granular understanding of the strength and character of the individual interactions between the ligand and the receptor.[34] During the docking analysis of all screened compounds with tryptase, each compound underwent individual scrutiny and scoring based on minimal docking energy values. This comprehensive evaluation aimed to identify compounds with favorable binding characteristics and promising interactions within the active site of tryptase (Table 2). The results revealed that several screened drugs demonstrate more negative docking energy scores as compared to the reference APC-366, emphasizing the potential superiority of the identified ligands. All the docket compounds are sorted according to the lowest docking energy values. Furthermore, these compounds already have known activities instead of tryptase and could be a possible inhibitor of tryptase too.

## SELECTION OF HIGHLY PREDICTED DRUGS

From the tryptase inhibitors identified through molecular docking analysis, the top seven drugs along with the reference compound APC-366 (Figure 4) were chosen for in-depth investigation. This included analyses of binding modes and experimental evaluation. Enalapril, a prodrug of enalaprilat, was also included in this selection. Although it did not rank highly in the predictive analysis, its selection was influenced by the


https://doi.org/10.1021/acsomega.4c04886
ACS Omega 2024, 9, 38820−38831

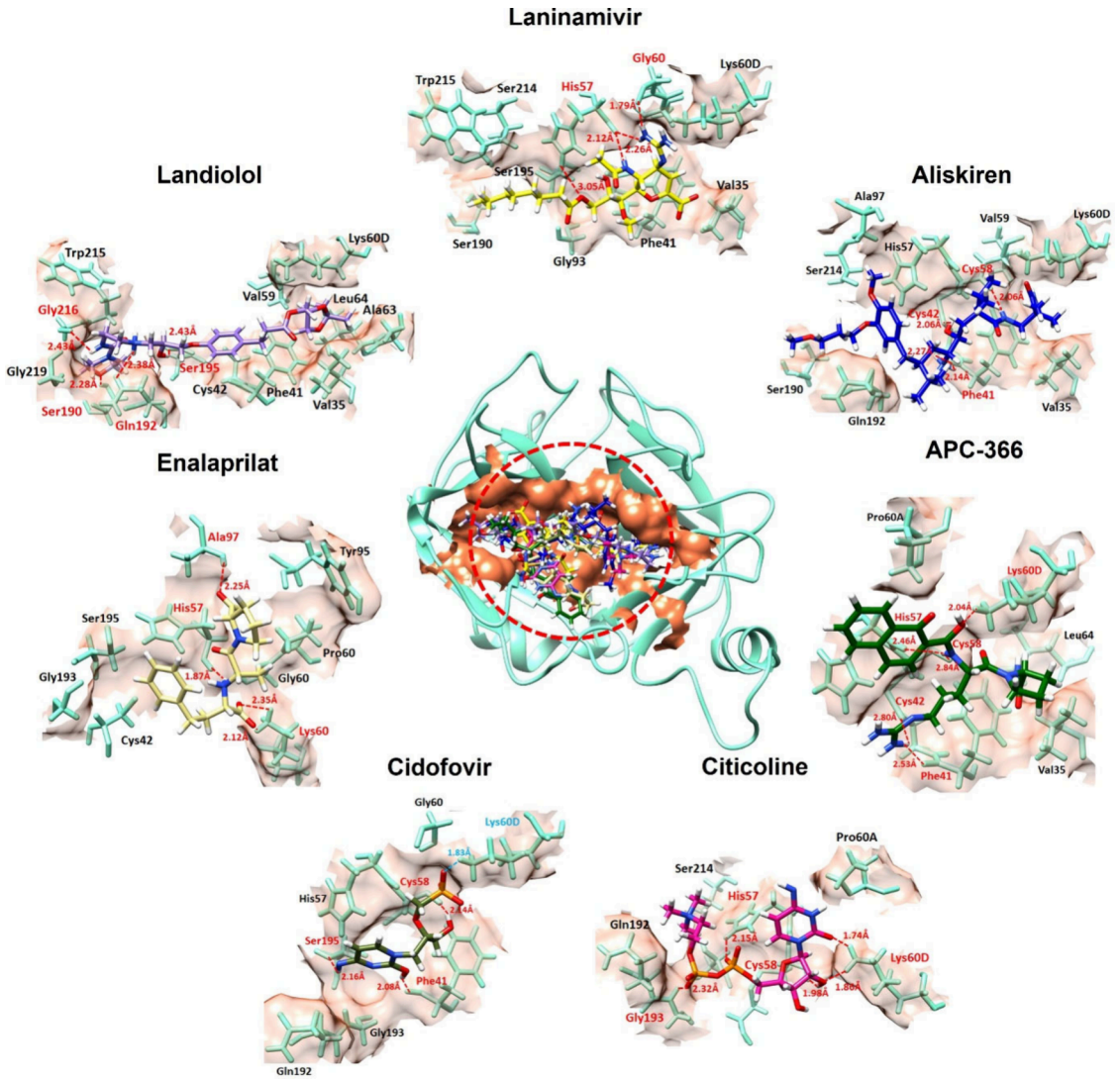


**Figure 5.** The 3D interactions between the ligand and the active region amino acids of tryptase. The hydrogen bond interaction and interacting amino acids are colored red, the salt bridges and salt bridge forming amino acids are colored cyan, and the other interacting amino acids are colored black.

practical consideration of enalaprilat's limited availability for experimental analysis. Laninamivir, known for inhibiting influenza neuraminidase, also appears to block tryptase, suggesting dual action that may enhance its antiviral effects. While neuraminidase inhibitors like laninamivir prevent virus spread by stopping the release of new viruses from cells, tryptase, released from mast cells, activates influenza hemagglutinin. This is significant, although some deadly influenza strains activate hemagglutinin differently. Our hypothesis about laninamivir's dual inhibition remains speculative, based on in vitro results, and requires further exploration to understand its full antiviral potential.

## BINDING INTERACTION ANALYSIS

The binding interaction analysis was conducted to discern the specific interactions and their types with the active region amino acid residues of the tryptase protein. This analysis aimed to determine whether the ligands bound effectively within the active binding pocket. Additionally, the identification of hydrogen bonds and salt bridges was part of this approach. The results indicated that APC-366, aliskiren, citocoline, cidofovir, enalaprilat, landiolol, and laninamivir successfully bound to the active binding pocket of the target protein, demonstrating favorable interactions as shown in Figure 5.

The APC-366 ligand−receptor complex demonstrates five hydrogen bonds with His57, Lys60, Cys58, Cys42, and Phe41. The oxygen atom of the ligand made a hydrogen bond with Lys60 with a bonding distance of 2.04 Å. A hydrogen atom of ligand formed two hydrogen bonds against His57 and Cys58 with bond lengths of 2.46 and 2.84 Å. Furthermore, another hydrogen atom formed two hydrogen bonds against Phe41 and Cys42 with bonding distances of 2.53 and 2.80 Å respectively. The aliskiren docking interaction analysis to the target protein exhibited that the ligand bind in the active region of the tryptase and manifested four hydrogen bonds with the active region amino acids. The four different hydrogen atoms of the ligand formed hydrogen bonds against Cys58, Cys42, and Phe41 with bonding distances of 2.06 Å, 2.06 Å, 2.27 Å, and 2.14 Å respectively.

The citocoline compound docked to tryptase demonstrated five hydrogen bonds against four different amino acids Lys60, His 57, Cys58, and Gly193. The two oxygen atoms of the


https://doi.org/10.1021/acsomega.4c04886
ACS Omega 2024, 9, 38820−38831

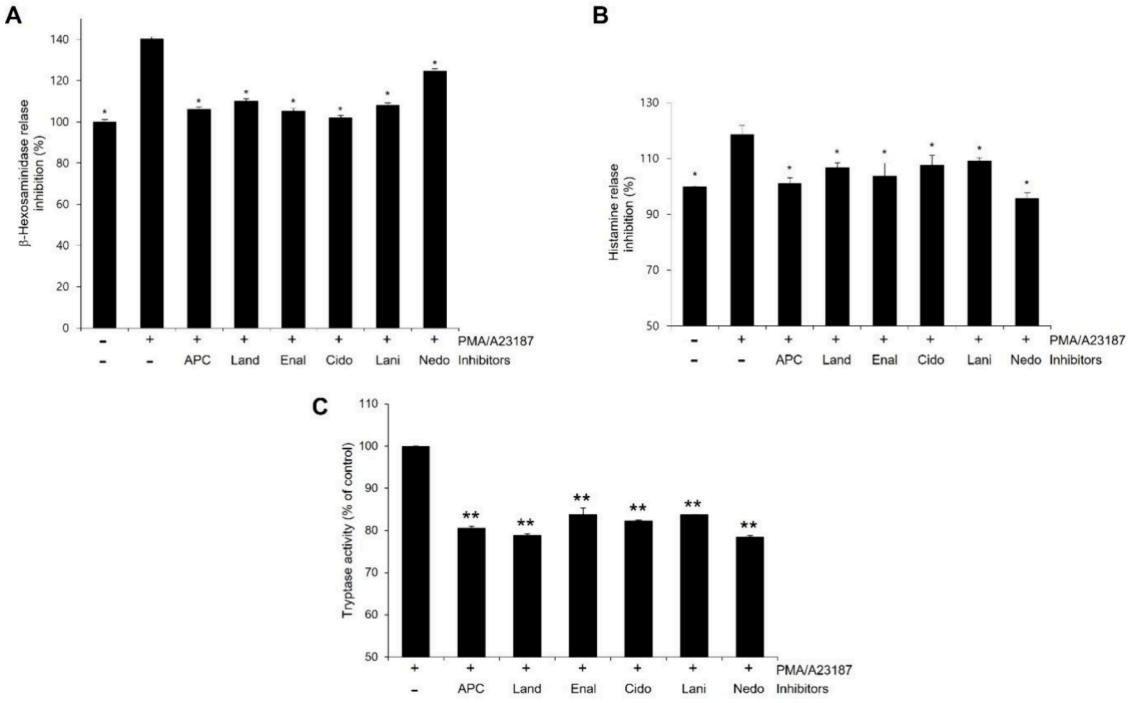


**Figure 6.** Inhibition of PMA/A23187-induced $\beta$-hexosaminidase activity (A), histamine release (B), and tryptase activity (C) in RBL-2H3 cells.

ligand form 2 hydrogen bonds with the same Lys60 with bonding distances of 1.74 Å, and 1.86 Å. Furthermore, two other oxygen atoms of ligand formed hydrogen bonds against His57 and Gly193 with bond lengths of 2.15 and 2.32 Å respectively. Moreover, the hydrogen atom of the ligand forms a hydrogen bond against Cys58 with a bond length of 1.98 Å. The cidofovir compound docked to tryptase depicted three hydrogen bonds and one salt bridge against the target protein. Two oxygen atoms of ligand formed two hydrogen bonds against Phe41 and Ser195 with bond lengths of 2.08 and 2.16 Å respectively. Furthermore, another hydrogen atom of the ligand formed a hydrogen bond against the binding pocket residues Cys58 with a bonding distance of 2.14 Å. Moreover, an oxygen atom of ligand formed a salt bridge against Lys60 with a bonding distance of 1.83 Å.

The enalaprilat-tryptase docked complex demonstrated three hydrogen bonds in the docking interaction analysis. Two different oxygen atoms of ligand formed two hydrogen bonds with different amino acid residues of binding pocket Ala97 and Lys60 with bond lengths of 2.25 and 2.35 Å respectively. Furthermore, a hydrogen atom of ligand formed a hydrogen bond against His57 with a bonding distance of 1.87 Å. Landiolol with a molecular weight of 509.6 g/mol occupied the extensive space in the active binding pocket of tryptase and exhibited four hydrogen bonds against the active region amino acids of the target protein. Three hydrogen atoms of landiolol formed hydrogen bonds against Ser195, Gln192, and Gly216 with bonding distances of 2.43 Å, 2.38 Å, and 2.43 Å respectively. Moreover, the oxygen atom of landiolol formed a hydrogen bond against Gly216 with a bonding distance of 2.43 Å. Laninamivir binds in the active region of tryptase and forms four hydrogen bonds against the active region of the target protein. The hydrogen atom of the ligand formed a hydrogen bond against Gly60 with a bond length of 1.79 Å. Furthermore, two hydrogen atoms formed two hydrogen bonds with the same amino acid residue His57 with bonding distances of 2.26 and 2.12 Å. Moreover, an oxygen atom of the ligand establishes a hydrogen bond with the aforementioned His57, with a bonding distance of 3.05 Å.

## EXPERIMENTAL VALIDATION

RBL-2H3 cell line, derived from rat basophilic leukemia cells, possess key characteristics with mast cells, notably the capacity to degranulate and release inflammatory mediators such as histamine and cytokines upon specific stimulation. This makes RBL-2H3 cells an optimal model for studying mast cell activation, signaling pathways, and the effects of various agents on mast cell functionality.[35,36] To induce mast cell activation, we exposed RBL-2H3 cells to known mast cell activators; phorbol myristate acetate (PMA) and calcium ionophore A23187. The effectiveness of activation was quantitatively assessed by measuring two primary markers of mast cell degranulation: the activity of $\beta$-hexosaminidase and the release of histamine. These markers are indicative of the degranulation process and the inflammatory response of mast cells. Additionally, in our experiments, we included nedocromil, an FDA-approved mast cell stabilizing agent, as a reference compound. The exact mechanism of action of nedocromil is not fully understood, but its established role in mast cell stabilization makes it a suitable reference. This was particularly pertinent given that APC-366 is an investigational tryptase inhibitor and there are currently no FDA-approved tryptase inhibitors available. Highly predicted drugs demonstrated significant suppression of both $\beta$-hexosaminidase activity (Figure 6A) and histamine release (Figure 6B) in RBL-2H3 cells challenged with PMA/A23187. These effects were observed to be similar in extent to those achieved by APC-366 and nedocromil. Most notably, the highly predicted drugs also significantly inhibited tryptase activity to the same extent as APC-366 and nedocromil (Figure 6C). Notably, tryptase inhibitors significantly reduced the release of histamine and $\beta$-hexosaminidase, in addition to inhibiting tryptase activity.


https://doi.org/10.1021/acsomega.4c04886
ACS Omega 2024, 9, 38820−38831

Previous studies have demonstrated that tryptase inhibitors, such as APC366-also used in our study-effectively decrease not only tryptase activity but also other markers of mast cell activation.[37,38] These findings suggest that tryptase may amplify mast cell activation, and its inhibition can consequently attenuate the overall mast cell response. However, additional research is needed to elucidate the specific mechanisms by which tryptase influences the degranulation process during mast cell activation. Nedocromil demonstrated a reduction in tryptase activity, which is likely attributable to its mast cell stabilizing properties, leading to decreased tryptase release, as opposed to a direct inhibitory effect on tryptase. This contrasts with other tested compounds that directly inhibited released tryptase during the mast cell activation process. These results are particularly significant as they suggest that these highly predicted drugs have the potential to serve as novel tryptase inhibitors.

## STRUCTURAL EVALUATION AND SIMILARITY COMPARISON

To evaluate the structural resemblance among the drugs that were highly predicted by both experimental and computational data, the Tanimoto similarity measure was applied using RDKit. This metric is crucial for comparing the similarity and diversity among compounds. The Tanimoto coefficient ranges from 0 to 1, where 0 indicates no similarity and 1 indicates complete similarity. Although there is no universally accepted threshold for similarity, a Tanimoto coefficient of 0.4 generally signifies a moderate level of similarity. This means the compounds share certain features but also possess significant differences (Figure S2A, and S2B)). With a Tanimoto similarity value around 0.4 certain drug groups were identified: APC-366, agatroban, and enalaprilat formed one group; laninamir and agatroban another; and citocholine, agatroban, and cidofovir yet another. Despite these groupings, no overarching similarity was found across all highly predicted drugs (Table S1).

Despite the limited overall similarity of the highly predicted drugs to APC-366, the possibility of shared specific structural features is still present. To investigate this further, the Maximum Common Substructure (MCS) algorithm was employed within RDKit, with a threshold of 0.5 set for the analysis. This led to the identification of common substructures among APC-366, agatroban, aliskiren, enalapril, and enalaprilat, which were highlighted in green color (Figure S2A). Notably, APC0366, argatroban, enalapril, and enalaprilat shared an N-(3-phenylproppyl) methylamine group in their structures, a feature absent in other drugs. This suggests that inhibitory activity against tryptase may involve factors beyond structural motifs, potentially including spatial arrangement or specific conformations. Additionally, similarity maps generated using RDKit's fingerprints assessed if the highly predicted drugs shared structural motifs with APC-366 (Figure S2B). The similarity maps revealed the extent to which APC-366's structural motif was present in the chemical structures of the highly predicted drugs. The insights gained from both MCS and similarity map analyses are instrumental in guiding further optimization of the drugs.

## METHODOLOGY

**Tryptase Inhibitor Reference Data Set and FDA-Approved Drug Library.** The reference data set of human tryptase inhibitor consists of 168 compounds, each with experimentally determined IC50 values. This data set was sourced from the ChEMBL database (https://www.ebi.ac.uk/chembl), specifically under the ChEMBL ID CHEMBL2095193. ChEMBL is a manually curated database known for its collection of bioactive molecules with drug-like properties. In the data set, all molecules are represented as canonicalized SMILES strings and IC50 values. For more efficient data representation and analysis, the IC50 values were converted to pIC50 values. The pIC50, which is the negative logarithm of the IC, ranges from 4.48 to 9.40. This corresponds to an IC range from 33,000 nM to 0.4 nM. Furthermore, an FDA-approved drug library was obtained from Selleck Chemicals (https://www.selleckchem.com). This library is comprised of 3,105 compounds. These FDA-approved drug molecules were initially in SDF (structure-data file) format and were converted to SMILES strings using RDKit.

**Molecular Descriptor Generation Using RDKit.** To evaluate the molecular properties of compounds, the RDKit (https://www.rdkit.org) platform was utilized. This open-source cheminformatics and machine learning framework, developed in Python, is adept at handling small molecule data. It offers a suite of features for processing and interpreting chemical structures, including tools for generating molecular descriptors, chemical features, and visualizing chemical data.[39] Therefore, the RDKit was employed to compute a set of nine molecular descriptors for both a tryptase reference data set and an FDA-approved drug library. These descriptors encompassed a range of molecular properties such as molecular weight, LogP value, number of hydrogen bond donors and acceptors, the proportion of sp3 hybridized carbon, the total number of aromatic bonds, ring count, topological polar surface area (TPSA), and the count of aromatic rings.

**Machine Learning Architecture.** The analysis of the tryptase reference data set incorporated machine learning techniques via scikit-learn (https://scikit-learn.org), a Python-based, open-source library designed for efficient and straightforward data analysis and mining. This library encompasses various algorithms for tasks such as regression, classification, clustering, dimensionality reduction, and model selection.[40] For this study, The data set was split into a training set and a test set in an 8:2 proportion. The molecular descriptors within the test set underwent training using the Random Forest Regression algorithm from the scikit-learn toolkit. Random Forest Regression, an ensemble learning approach, aggregates the outputs of numerous decision trees to enhance the model's precision and reliability (https://scikit-learn.org/stable/modules/generated/sklearn.ensemble.RandomForestRegressor.html). Upon completion of the training phase with the training data set, the model's accuracy was evaluated using the test data set, focusing on metrics like mean squared error and the regression coefficient. Additionally, the relative influence of each descriptor was quantified through feature importance values.[41,42] To predict pIC50 values for the FDA-approved drug data set, we calculated its molecular descriptors using RDkit as with the tryptase reference data set and then applied these molecular descriptors to the Random Forest Regression model.

**Tryptase Structure Retrieval.** Human beta 2 tryptase (TPSB2) exists in a tetrameric form, composed of four identical subunits. The 3D structure of tryptase protein was examined using the A subunit from the crystal structure


https://doi.org/10.1021/acsomega.4c04886
ACS Omega 2024, 9, 38820−38831

identified as PDBID: 2GDD, which has a resolution of 2.35 Å, from the Protein Data Bank (PDB) (https://www.rcsb.org/structure/2GDD). To refine the structure for the analyses, energy minimization was employed using UCSF Chimera software. The tryptase protein, composed of $\alpha$-helices, $\beta$-sheets, and turns, underwent a quantitative analysis of its structure using the VADAR (http://vadar.wishartlab.com/) Internet server.[43] Additionally, the Ramachandran plots were generated using Discovery Studio.[44] Moreover, the same tool was utilized to investigate the 3D structure of the protein.

**Prediction of Active Binding Site.** The placement of a ligand within the protein's holo-structure is a strong indicator of the targeted protein's binding pocket.[45,46] The tryptase inhibitor complex was obtained from the PDB (PDB ID: 2GDD). To ensure the precision of binding site selection, interacting amino acids were chosen using the ligand interaction feature of Discovery Studio. As a result, the cocrystallized ligand was selected, and the binding sphere was established using the current selection method within the define binding site window of Discovery Studio. Subsequently, the binding sphere was reduced to be confined to the chosen amino acids.

**Molecular Docking.** Molecular docking stands as one of the most extensively employed methods for assessing the interactions and conformations of ligands with target proteins.[47,48] Certainly, scoring algorithms in molecular docking enable the estimation of association strength or binding affinity between two molecules by assessing their preferred orientation. This predictive capability enhances our understanding of molecular interactions and aids in identifying potential ligands for target proteins.[33] The protein underwent preparation steps before molecular docking, involving the removal of water molecules and the cocrystallized ligand by UCSF Chimera. Additionally, hydrogen atoms were added to the protein using Discovery Studio's protein preparation approach. Ligand preparations for both screened and reference compounds were conducted, involving tautomer generation, ionization adjustments, and addressing bad valencies through Discovery Studio's ligands preparation module. Subsequently, the CDOCKER module of Discovery Studio was utilized to carry out molecular docking of the screened FDA candidate compounds against tryptase, with default orientation and conformation settings at 10/10. Each chosen compound underwent molecular docking against tryptase, and the top hits were selected based on the lowest binding energy values (in kcal/mol) to identify the best-docked complexes.

**Binding Interaction Analysis.** The top docked complexes, along with APC-366 as a reference drug, were subjected to three-dimensional (3D) graphical analysis using UCSF Chimera[49] and Discovery Studio. This analysis aimed to comprehensively study the interactions between ligands and the target protein, providing insights into the spatial arrangement and binding characteristics of the compounds within the protein's active site.

**Experimental Reagents and Cell Culture.** Cidofovir dihydrate was acquired from GLPBIO (#GC13936, MONTCLAIR, USA). All other chemicals required for the experiment were procured from Sigma-Aldrich, located in St. Louis, MO, USA. The RBL-2H3 cells were acquired from the Korea cell line bank (KCLB), with the catalog number 22256 (RBL-2H3). The RBL-2H3 cells were cultured in RPMI 1640 medium (Hyclon Laboratories), supplemented with 10% heat-inactivated fetal bovine serum and 100 U/ml of penicillin-streptomycin (Gibco). The cells were maintained at 37 °C in an atmosphere containing 5% $CO_2$.

**$\beta$-Hexosaminidase ($\beta$-HEX) Activity and Histamine Release Assay.** To assess the impact of chemicals on degranulation, we quantified the levels of $\beta$-HEX activity and histamine release. This enzyme is found within the granules of mast cells and is commonly used as a marker for granule content.[50] RBL-2H3 cells were grown in 12-well plates for a duration of 24 h. The medium was then discarded, and the cells were treated with 0.1 $\mu$M of inhibitors diluted in PIPES buffer for 1 h at 37 °C. Following this pretreatment, the cells were washed twice with PIPES buffer and subsequently stimulated with 50 nM of PMA and 1 $\mu$M of A23187 for 30 min at 37 °C. A 20 $\mu$L aliquot of the supernatant was then allowed to react with 80 $\mu$L of substrate buffer (containing 2 mM 4-p-nitrophenyl-N-acetyl-$\beta$-D-glucosaminide in 0.05 M sodium citrate buffer, pH 4.5) for 30 min at 37 °C. The reaction was halted by the addition of 200 $\mu$L of stop buffer (0.1 M NaHCO3, pH 10). The absorbance was measured at 405 nm using a microplate spectrophotometer (SpectraMax M5, Molecular Devices, USA). The concentration of histamine was determined using the o-phthalaldehyde (OPT) spectrofluorometric method.[51] To each well's 0.5 mL of supernatant, 0.1 mL of 1 M NaOH and 25 $\mu$L of OPT (1% weight/volume in methanol) were added. The mixture was then incubated for 4 min at room temperature. The reaction was terminated by adding 50 $\mu$L of 3 M HCl. The absorbance was measured at excitation and emission wavelengths of 360 and 450 nm, respectively, using a microplate spectrophotometer (SpectraMax M5, Molecular Devices, USA).

**Tryptase Inhibition Activity Assay.** Tryptase activity was measured using the Tryptase Activity Assay kit from Tribioscience (#TBS2101, Tribioscience, USA) following the manufacturer's instructions. To prepare cellular tryptase, RBL-2H3 cells were detached from the culture plate. After detaching the cells, wash them and adjust the cell concentration to 1.0 × 107 cells/mL with 1X assay buffer. The suspended cells were incubated in the presence of the 0.1 $\mu$M of inhibitors for 1 h and then stimulated with 50 nM of PMA and 1 $\mu$M of A23187 for 30 min at 37 °C in a 5% CO2 incubator. The cell suspension was centrifuged at 700 X g, and the supernatant was carefully collected. For the tryptase inhibition activity assay, the assay mixture was made by adding 50 $\mu$L of supernatant to 130 $\mu$L of assay buffer. The colorimetric reaction was initiated by adding 20 $\mu$L of the tryptase substrate. The reactions were observed at 405 nm in kinetic mode for a duration of 60 min at 37 °C using a microplate spectrophotometer (Molecular Devices, San Jose, CA, USA). Each assay was conducted in triplicate.

**Statistical Analysis.** All values presented in the figures are depicted as the mean ± standard deviation (SD), derived from a minimum of three independent experiments. Statistical significance was determined using a two-tailed Student's $t$ test. Data with $p$-values less than 0.05 were considered statistically significant. Single (*) and double (**) asterisks indicate statistical significance at $p < 0.05$ and $p < 0.01$, respectively.

## CONCLUSION

The increasing duration and cost of drug development necessitate the exploration of emerging techniques to streamline this process. Machine learning (ML) has emerged as a particularly effective tool in identifying lead compounds with high potential for successful drug development. Our study


https://doi.org/10.1021/acsomega.4c04886
ACS Omega 2024, 9, 38820−38831

demonstrates the distinct advantages of ML-based screening in terms of efficiency and high throughput performance in drug design.

In our research, compounds predicted by ML to be effective were selected from FDA-approved drugs. These compounds were shown to fit well within the active region of tryptase, effectively blocking its active site in computational models. Further validation was provided through biological assessment of these compounds. The activities of these highly predicted drugs were comparable to the reference compound APC-366, underscoring their potential efficacy as tryptase inhibitors. Although numerous tryptase inhibitors have been previously reported, it is important to note that these are largely in investigational stages and have not yet received FDA approval. Notably, the fact that these compounds are already FDA-approved adds feasibility and safety to their potential use. Therefore, our study concludes that ML-based drug screening, particularly in the context of drug repurposing, presents a promising approach for the development of novel tryptase inhibitors, offering a significant contribution to the field of drug discovery.

## ■ ASSOCIATED CONTENT

### Data Availability Statement

The data supporting the findings of this study are available upon reasonable request from the corresponding author. All the data that support the findings of this study are available in the Supporting Information and GitHub repository (https://github.com/Yasirubunt/Tryptase_Project).

### Supporting Information

The Supporting Information is available free of charge at https://pubs.acs.org/doi/10.1021/acsomega.4c04886.

Figure S1 is the 3D structure of the tryptase, Ramachandran plot, Coulombic surface area, and amino acid sequence; Figure S2 is a graphical representation of common structural motif found with Maximum Common Substructure and the similarity maps of the screened compounds; Table S1 is a Tanimoto similarity comparison of APC-366 and screened tryptase inhibitors; and machine learning data sets, Molecular Docking file, and docked complexes available in the GitHub repository (PDF)

## ■ AUTHOR INFORMATION


### Corresponding Author

**Wanjoo Chun** − *Department of Pharmacology, Kangwon National University School of Medicine, Chuncheon 24341, Republic of Korea;* orcid.org/0000-0003-1984-3545; Phone: +82-33-250-8853; Email: wchun@kangwon.ac.kr

### Authors

**Muhammad Yasir** − *Department of Pharmacology, Kangwon National University School of Medicine, Chuncheon 24341, Republic of Korea*

**Jinyoung Park** − *Department of Pharmacology, Kangwon National University School of Medicine, Chuncheon 24341, Republic of Korea*

**Eun-Taek Han** − *Department of Medical Environmental Biology and Tropical Medicine, Kangwon National University School of Medicine, Chuncheon 24341, Republic of Korea*

**Won Sun Park** − *Department of Physiology, Kangwon National University School of Medicine, Chuncheon 24341, Republic of Korea*

**Jin-Hee Han** − *Department of Medical Environmental Biology and Tropical Medicine, Kangwon National University School of Medicine, Chuncheon 24341, Republic of Korea*

Complete contact information is available at: https://pubs.acs.org/10.1021/acsomega.4c04886


### Author Contributions

MY and JYP contributed equally to this work. MY and JYP were involved in the experimental operation and data analysis. ETH, WSP, and JHH were involved in data curation and the methodology. MY and JYP were involved in the writing of the manuscript. WC was involved in the conceptualization, reviewing, and editing of the manuscript. WC confirmed the authenticity of all the raw data. All authors have read and approved the final manuscript.

### Notes

The authors declare no competing financial interest.

## ■ ACKNOWLEDGMENTS

We acknowledge the funding support from the Institute of Medical Sciences, Kangwon National University, 2024.

## ■ REFERENCES


(1) Palma, A. M.; Hanes, M. R.; Marshall, J. S. J. F. i. I. Mast cell modulation of b cell responses: An under-appreciated partnership in host defence. *Front Immunol* **2021**, *12*, 718499.

(2) Dileepan, K. N.; Raveendran, V. V.; Sharma, R.; Abraham, H.; Barua, R.; Singh, V.; Sharma, R.; Sharma, M. J. F. i. M., Mast cell-mediated immune regulation in health and disease, *Front Med. (Lausanne)* **2023**, *10*, DOI: 10.3389/fmed.2023.1213320.

(3) Banafea, G. H.; Bakhashab, S.; Alshaibi, H. F.; Natesan Pushparaj, P.; Rasool, M. J. B. The role of human mast cells in allergy and asthma. *Bioengineered* **2022**, *13* (3), 7049−7064.

(4) Paivandy, A.; Pejler, G. J. J. o. I. I. Novel strategies to target mast cells in disease. *J. Innate Immun* **2021**, *13* (3), 131−147.

(5) Elieh Ali Komi, D.; Wöhrl, S.; Bielory, L. J. C. r. i. a. immunology, Mast cell biology at molecular level: a comprehensive review. *Clin Rev. Allergy Immunol* **2020**, *58*, 342−365.

(6) Vitte, J.; Vibhushan, S.; Bratti, M.; Montero-Hernandez, J. E.; Blank, U. J. M. P. Practice, Allergy, anaphylaxis, and nonallergic hypersensitivity: IgE, mast cells, and beyond. *Med. Princ Pract* **2023**, *31* (6), 501−515.

(7) Voss, M.; Kotrba, J.; Gaffal, E.; Katsoulis-Dimitriou, K.; Dudeck, A. Mast cells in the skin: defenders of integrity or offenders in inflammation? *Int. J. Mol. Sci.* **2021**, *22* (9), 4589.

(8) Karimi, N.; Morovati, S.; Chan, L.; Napoleoni, C.; Mehrani, Y.; Bridle, B. W.; Karimi, K. J. B. Mast cell tryptase and implications for SARS-CoV-2 pathogenesis. *BioMed.* **2021**, *1* (2), 136−149.

(9) Giardina, S. F.; Werner, D. S.; Pingle, M.; Feinberg, P. B.; Foreman, K. W.; Bergstrom, D. E.; Arnold, L. D.; Barany, F. J. J. o. M. C. Novel, self-assembling dimeric inhibitors of human $\beta$ tryptase. *J. Med. Chem.* **2020**, *63* (6), 3004−3027.

(10) Lyons, J. J.; Yi, T. J. C. O. i. I. Mast cell tryptases in allergic inflammation and immediate hypersensitivity. *Curr. Opin Immunol* **2021**, *72*, 94−106.

(11) Carvalho, N.; Carolino, E.; Ferreira, M.; Coelho, H.; Santos, C. R.; Barreira, A. L.; Henriques, S.; Cardoso, C.; Moita, L.; Costa, P. M. Tryptase in Acute Appendicitis: Unveiling Allergic Connections through Compelling Evidence. *Int. J. Mol. Sci.* **2024**, *25* (3), 1645.

(12) Michel, M.; Klingebiel, C.; Vitte, J. J. A. o. A. Asthma; Immunology, Tryptase in type I hypersensitivity. *Ann. Allergy Asthma Immunol* **2023**, *130* (2), 169−177.

(13) Ma, C.; Li, H.; Lu, S.; Li, X.; Wang, S.; Wang, W. J. J. o. I. R. Tryptase and Exogenous Trypsin: Mechanisms and Ophthalmic Applications. *J. Inflam Res.* **2023**, *16*, 927−939.
(14) Parvathaneni, V.; Kulkarni, N. S.; Muth, A.; Gupta, V. J. D. d. t. Drug repurposing: a promising tool to accelerate the drug discovery process. *Drug Discov Today* **2019**, *24* (10), 2076−2085.
(15) Roy, S.; Dhaneshwar, S.; Bhasin, B. Drug repurposing: an emerging tool for drug reuse, recycling and discovery. *Curr. Drug Discov* **2021**, *13* (2), 101−119.
(16) Küçükkeles, B. Practicing Repurposing in the Pharmaceutical Industry: Uncovering New Uses for Potential Resources. ETH Zurich, **2019**. DOI: 10.3929/ethz-b-000404107.
(17) Low, Z. Y.; Farouk, I. A.; Lal, S. K. J. V. Drug repositioning: new approaches and future prospects for life-debilitating diseases and the COVID-19 pandemic outbreak. *Viruses* **2020**, *12* (9), 1058.
(18) Farha, M. A.; Brown, E. D. J. N. m. Drug repurposing for antimicrobial discovery. *Nat. Microbiol* **2019**, *4* (4), 565−577.
(19) Sabe, V. T.; Ntombela, T.; Jhamba, L. A.; Maguire, G. E.; Govender, T.; Naicker, T.; Kruger, H. G. Current trends in computer aided drug design and a highlight of drugs discovered via computational techniques: A review. *Eur. J. Med. Chem.* **2021**, *224*, 113705.
(20) Niazi, S. K.; Mariam, Z. J. P. Computer-aided drug design and drug discovery: a prospective analysis. *Pharmaceuticals* **2024**, *17* (1), 22.
(21) Macalino, S. J. Y.; Gosu, V.; Hong, S.; Choi, S. J. A. o. p. r. Role of computer-aided drug design in modern drug discovery. *Arch Pharm. Res.* **2015**, *38*, 1686−1701.
(22) Rahman, M. M.; Islam, M. R.; Rahman, F.; Rahaman, M. S.; Khan, M. S.; Abrar, S.; Ray, T. K.; Uddin, M. B.; Kali, M. S. K.; Dua, K. J. B.; et al. Emerging promise of computational techniques in anti-cancer research: at a glance. *Bioengineering* **2022**, *9* (8), 335.
(23) Basith, S.; Cui, M.; Macalino, S. J.; Choi, S. J. C. m. c. Expediting the design, discovery and development of anticancer drugs using computational approaches. *Curr. Med. Chem.* **2018**, *24* (42), 4753−4778.
(24) Gupta, R.; Srivastava, D.; Sahu, M.; Tiwari, S.; Ambasta, R. K.; Kumar, P. J. M. d. Artificial intelligence to deep learning: machine intelligence approach for drug discovery. *Mol. Divers* **2021**, *25*, 1315−1360.
(25) Alzubi, J.; Nayyar, A.; Kumar, A. In *Machine Learning from Theory to Algorithms: An Overview*; Journal of Physics: Conference Series, IOP Publishing, 2018; p 012012.
(26) Aniche, M.; Maziero, E.; Durelli, R.; Durelli, V. H. S. The effectiveness of supervised machine learning algorithms in predicting software refactoring. *IEEE Transact Soft Eng.* **2020**, *48* (4), 1432−1450.
(27) Singh, S.; Kumar, R.; Payra, S.; Singh, S. K. J. C. Artificial Intelligence and Machine Learning in Pharmacological Research: Bridging the Gap between Data and Drug Discovery. *Cureus* **2023**, *15* (8), DOI: 10.7759/cureus.44359.
(28) Vamathevan, J.; Clark, D.; Czodrowski, P.; Dunham, I.; Ferran, E.; Lee, G.; Li, B.; Madabhushi, A.; Shah, P.; Spitzer, M. J. N. r. D. d. Applications of machine learning in drug discovery and development. *Nat. Rev. Drug Discov* **2019**, *18* (6), 463−477.
(29) Rigatti, S. J. Random forest. *J. Insur Med.* **2017**, *47* (1), 31−39.
(30) Jaganathan, K.; Tayara, H.; Chong, K. T. J. P. An explainable supervised machine learning model for predicting respiratory toxicity of chemicals using optimal molecular descriptors. *Pharmaceutics* **2022**, *14* (4), 832.
(31) Lind, A. P.; Anderson, P. C. J. P. o. Predicting drug activity against cancer cells by random forest models based on minimal genomic information and chemical properties. *PLoS One* **2019**, *14* (7), No. e0219774.
(32) Atiakshin, D.; Buchwalow, I.; Samoilova, V.; Tiemann, M. J. H.; biology, c. Tryptase as a polyfunctional component of mast cells. *Histochem Cell Biol.* **2018**, *149* (5), 461−477.
(33) Yasir, M.; Park, J.; Han, E.-T.; Park, W. S.; Han, J.-H.; Kwon, Y.-S.; Lee, H.-J.; Hassan, M.; Kloczkowski, A.; Chun, W. J. M. Exploration of Flavonoids as Lead Compounds against Ewing Sarcoma through Molecular Docking, Pharmacogenomics Analysis, and Molecular Dynamics Simulations. *Molecules* **2023**, *28* (1), 414.
(34) Yasir, M.; Park, J.; Lee, Y.; Han, E. T.; Park, W. S.; Han, J. H.; Kwon, Y. S.; Lee, H. J.; Chun, W. Discovery of GABA Amino-transferase Inhibitors via Molecular Docking, Molecular Dynamic Simulation, and Biological Evaluation. *Int. J. Mol. Sci.* **2023**, *24* (23), 16990.
(35) Passante, E.; Frankish, N. J. I. R. The RBL-2H3 cell line: its provenance and suitability as a model for the mast cell. *Inflamm Res.* **2009**, *58*, 737−745.
(36) Do, H. J.; Oh, T. W.; Yang, J. H.; Park, K. I.; Ma, J. Y. Davallia mariesii moore improves FcεRI-mediated allergic responses in the rat basophilic leukemia mast cell line RBL-2H3 and passive cutaneous anaphylaxis in mice. *Mediators Inflamm* **2017**, *2017*, 1.
(37) He, S.; Gaça, M. D.; Walls, A. F. Therapeutics, A role for tryptase in the activation of human mast cells: modulation of histamine release by tryptase and inhibitors of tryptase. *J. Pharmacol Exp Ther* **1998**, *286* (1), 289−297.
(38) He, S.; McEuen, A. R.; Blewett, S. A.; Li, P.; Buckley, M. G.; Leufkens, P.; Walls, A. F. J. B. p. The inhibition of mast cell activation by neutrophil lactoferrin: uptake by mast cells and interaction with tryptase, chymase and cathepsin G. *Biochem. Pharmacol.* **2003**, *65* (6), 1007−1015.
(39) Landrum, G. J. R. Rdkit documentation. 2013, *1* (1−79), 4, https://www.rdkit.org/RDKit_Docs.2011_12_1.pdf.
(40) Pedregosa, F.; Varoquaux, G.; Gramfort, A.; Michel, V.; Thirion, B.; Grisel, O.; Blondel, M.; Prettenhofer, P.; Weiss, R.; Dubourg, V. Scikit-learn: Machine learning in Python. *JMLR* **2011**, *12*, 2825−2830.
(41) Yasir, M.; Park, J.; Han, E. T.; Park, W. S.; Han, J. H.; Kwon, Y. S.; Lee, H. J.; Chun, W. Machine Learning-Based Drug Repositioning of Novel Janus Kinase 2 Inhibitors Utilizing Molecular Docking and Molecular Dynamic Simulation. *J. Chem. Inf Model* **2023**, *63* (21), 6487−6500.
(42) Yasir, M.; Park, J.; Han, E.-T.; Park, W. S.; Han, J.-H.; Kwon, Y.-S.; Lee, H.-J.; Chun, W. Vismodegib Identified as a Novel COX-2 Inhibitor via Deep-Learning-Based Drug Repositioning and Molecular Docking Analysis. *ACS Omega* **2023**, *8* (37), 34160−34170.
(43) Willard, L.; Ranjan, A.; Zhang, H.; Monzavi, H.; Boyko, R. F.; Sykes, B. D.; Wishart, D. S. J. N. a. r. VADAR: a web server for quantitative evaluation of protein structure quality. *Nucleic Acids Res.* **2003**, *31* (13), 3316−3319.
(44) *Discovery Studio*; Discovery Studio, 2008.
(45) Hassan, M.; Yasir, M.; Shahzadi, S.; Kloczkowski, A. J. A. o. Exploration of Potential Ewing Sarcoma Drugs from FDA-Approved Pharmaceuticals through Computational Drug Repositioning, Pharmacogenomics, Molecular Docking, and MD Simulation Studies. *ACS Omega* **2022**, *7* (23), 19243−19260.
(46) Yasir, M.; Park, J.; Han, E. T.; Park, W. S.; Han, J. H.; Kwon, Y. S.; Lee, H. J.; Chun, W. Computational Exploration of Licorice for Lead Compounds against Plasmodium vivax Duffy Binding Protein Utilizing Molecular Docking and Molecular Dynamic Simulation. *Molecules (Basel, Switzerland)* **2023**, *28* (8), 3358.
(47) Yasir, M.; Park, J.; Han, E. T.; Park, W. S.; Han, J. H.; Kwon, Y. S.; Lee, H. J.; Hassan, M.; Kloczkowski, A.; Chun, W. Investigation of Flavonoid Scaffolds as DAX1 Inhibitors against Ewing Sarcoma through Pharmacoinformatic and Dynamic Simulation Studies. *Int. J. Mol. Sci.* **2023**, *24* (11), 9332.
(48) Naqvi, A. A.; Mohammad, T.; Hasan, G. M.; Hassan, M. I. Advancements in docking and molecular dynamics simulations towards ligand-receptor interactions and structure-function relationships. *Curr. Top Med. Chem.* **2018**, *18* (20), 1755−1768.
(49) Pettersen, E. F.; Goddard, T. D.; Huang, C. C.; Couch, G. S.; Greenblatt, D. M.; Meng, E. C.; Ferrin, T. E. UCSF Chimera—a visualization system for exploratory research and analysis. *J. Comput. Chem.* **2004**, *25* (13), 1605−1612.


https://doi.org/10.1021/acsomega.4c04886
*ACS Omega* 2024, 9, 38820−38831

(50) Schwartz, L. B.; Lewis, R. A.; Seldin, D.; Austen, K. F. Acid hydrolases and tryptase from secretory granules of dispersed human lung mast cells. *J. Immunol* **1981**, *126* (4), 1290−4.
(51) Passante, E.; Ehrhardt, C.; Sheridan, H.; Frankish, N. RBL-2H3 cells are an imprecise model for mast cell mediator release. *Inflammation research* **2009**, *58* (9), 611−8.



https://doi.org/10.1021/acsomega.4c04886
*ACS Omega* 2024, 9, 38820−38831